EES Catalysis

PAPER

View Article Online
View Journal

Cite this: DOI: 10.1039/d5ey00333d

Industrial amine blends enable efficient CO electrosynthesis in reactive capture

Siyu Sonia Sun, †[a] Yurou Celine Xiao, †[a] Feng Li,[a] Jinhong Wu,[a] Yuxuan Che,[a] Yong Wang,[a] Min Liu,[a] Yaohao Guo,[a] Mengyang Fan,[a] Kai Han,[b] Paul-Emmanuel Just,[b] Paul J. Corbett,[b] Rui Kai Miao*[a] and David Sinton*[a]

Received 18th November 2025,
Accepted 5th December 2025

DOI: 10.1039/d5ey00333d

rsc.li/eescatalysis

Reactive capture of CO_2 (RCC) integrates CO_2 capture and electrochemical conversion into carbon monoxide (CO), avoiding the energy-intensive CO_2 regeneration required in conventional CO_2 electrolysis. While single-component amines have been used in prior RCC systems, they suffer from limited CO energy efficiency (<15%) due to sluggish CO_2 release. In contrast, the norm in industrial CO_2 capture is to blend amines for a favorable combination of absorption rate, CO_2 loading capacity, and release energetics. Here, we explore whether blending amines could likewise benefit reactive capture. Using aqueous blends of monoethanolamine (MEA) and methyldiethanolamine (MDEA), we find a strong correlation between bicarbonate concentration in the post-capture solution and CO faradaic efficiency (FE). However, under industrial absorption conditions, the blend with the highest bicarbonate content did not always yield the best CO FE: although MDEA increased bicarbonate concentrations, it also increased the viscosity, hindering CO_2 mass transport and increasing cell resistance. These competing effects highlight that, for efficient RCC, the composition must balance CO_2 absorption kinetics and capacity for capture, as well as CO_2 availability and transport properties for conversion. Screening the performance of binary and commercial amine blends, we find a CO energy efficiency (EE) of 31% at 50 mA cm^{-2}—a 2.4-fold improvement over single-amine systems.

Broader context

Capturing CO_2 from point sources and deploying efficient utilization strategies help to mitigate the climate crisis. Conventional solvent-based capture is energy-intensive, with thermal regeneration accounting for most of the operating cost. Electrochemical CO_2 conversion powered by low-carbon electricity is attractive but relies on purified gaseous CO_2, reintroducing the same regeneration bottleneck. Reactive CO_2 capture (RCC) integrates capture and electrolysis by feeding CO_2-rich solvents directly into an electrolyzer, where an electrochemically driven pH swing releases CO_2 *in situ* for reduction, bypassing energy-intensive regeneration. The choice of capture media is critical for RCC. Industrial CO_2 capture commonly employs amine blends that pair fast-absorbing activators (primary/secondary amines) with low-regeneration-energy promoters (tertiary amines) to balance absorption kinetics, capacity, and release energetics. Translating this design principle to RCC may similarly optimize both capture and conversion performance. Here, we show that amine blending in RCC systems enhances CO selectivity and energy efficiency compared to single-amine solvents, while revealing the need to balance favorable speciation with transport properties such as increased viscosity.

Introduction

Capturing carbon dioxide (CO_2) from flue gas streams and converting it *via* electrochemical CO_2 reduction reaction (CO_2RR) presents a promising strategy to mitigate CO_2 emissions while generating useful fuels and chemicals.[1,2] Conventional CO_2 capture methods rely on solution absorption, which demands substantial thermal energy to regenerate the capture solution and produce pure gaseous CO_2 for sequestration or conversion.[3,4] RCC offers a more energy-efficient alternative by directly converting the CO_2-rich capture solution in an electrolyzer, bypassing energy-intensive thermal regeneration.[5,6]

In an RCC system, CO_2 from flue gas is captured in an absorber and the resulting CO_2-rich solution is then fed directly into an electrolyzer and reduced into value-added chemicals such as carbon monoxide (CO), while the capture solution is simultaneously regenerated and recirculated back to the absorber to complete the cycle (Fig. 1).

[a] Department of Mechanical and Industrial Engineering, University of Toronto, Ontario, Canada. E-mail: sinton@mie.utoronto.ca, ruikai.miao@mail.utoronto.ca
[b] Shell Global Solutions International B.V., Amsterdam, the Netherlands
† These authors contributed equally to this work.

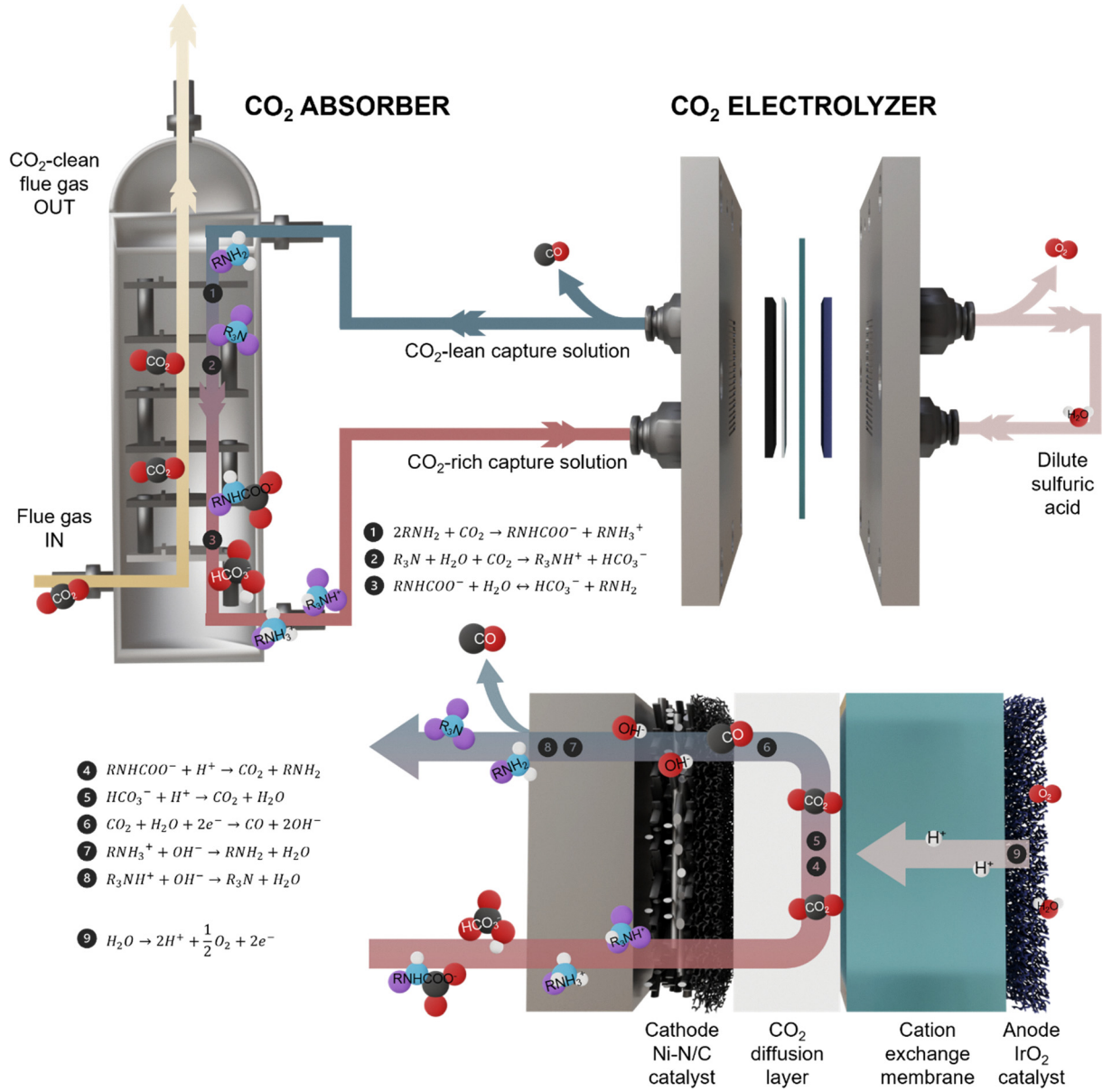

Fig. 1 Schematic of the reactive capture system using amine blends as capture solution.

Several capture solutions have been explored for RCC targeting CO. Alkali hydroxides capture CO_2 with rapid kinetics at high pH (>12), forming alkali carbonate, but protonating alkali carbonate to CO_2 for conversion requires two electron-coupled protons, limiting the theoretical CO faradaic efficiency (FE) to 50%.[7–10] In contrast, alkali carbonates capture CO_2 in the form of alkali bicarbonate that only requires one electron-coupled proton to release, enabling up to 100% theoretical CO FE.[11] However, carbonate-based systems exhibit sluggish CO_2 absorption kinetics, necessitating larger absorber units to achieve sufficient uptake, increasing the cost of capture.[12] To improve capture kinetics, promoter additives like glycine are often introduced to accelerate CO_2 absorption, but these additives lower CO FE during electrolysis.[13–15]

Capture solutions for RCC must combine rapid CO_2 absorption with facile release for conversion. Amine-based solutions meet this need: they absorb CO_2 at rates exceeding those of alkali carbonates and form carbamate and bicarbonate species.[16,17] However, primary amines, such as monoethanolamine (MEA), form stable CO_2-adducts that make CO_2 release energetically demanding.[18,19] Recent advances in reactive capture amines have established two complementary operating regimes: systems in which piperazine (PZ) carbamates are directly reduced to CO,[20] and systems in which electrolysis proceeds *via in situ* protonation of carbamates and bicarbonates (both of which require just one electron-coupled proton for CO_2 release).[17,21] Direct carbamate reduction is attractive because it can, in principle, bypass CO_2 desorption, but carbamate is a strongly bound, low-mobility species, making it intrinsically more difficult to reduce and typically requiring elevated temperatures and higher overpotentials.[19] In this work, we focus on the *in situ* regeneration regime, where proton-assisted

conversion of chemisorbed species to dissolved CO_2 provides a local CO_2 reservoir at the catalyst interface and is compatible with established CO_2 reduction catalysts and cell architectures that can operate at industrial-relevant current densities. We use industrially relevant amine blends—combinations of "activator" amines (primary/secondary) and "promoter" amines (tertiary/hindered)—to balance fast absorption kinetics from activators and low-energy CO_2 releases from promoters.[22] In this context, we investigate the potential of blended amines to achieve both rapid CO_2 absorption and high CO selectivity in RCC systems.

Correlation between post-capture species and electrolysis performance

To explore the feasibility of using amine blends for RCC, we focus initially on MEA and methyldiethanolamine (MDEA) as a well-established industrial activator–promoter pair.[23] We employed a zeolitic imidazolate framework (ZIF)-8-derived nickel single-atom catalyst (Ni–N/C, Fig. S1 and S2) following established methods, which has previously demonstrated high CO selectivity in amine-based RCC systems.[10,21]

We evaluated MEA, MDEA and their blends as reactive capture solutions. To ensure a fair comparison, we attempted to control CO_2 purging so that all blended solutions reached an identical loading of 0.56 mol_{CO_2} mol_{amine}^{-1}, a typical industrial CO_2 loading for 5 M MEA.[24] However, the 5 M MDEA solution exhibited substantially slower CO_2 absorption, requiring four times longer than the MEA/MDEA blend to reach even half of the target loading (0.29 mol_{CO_2} mol_{amine}^{-1}). The absorption rate of the 5 M MDEA declined over time and plateaued, suggesting that MDEA alone is ineffective as a capture medium (Fig. S3). At 50 mA cm^{-2}, we achieved a CO FE of 40% using the 5 M MEA solution, and 59% using a 2.5 M MEA + 2.5 M MDEA blend at the target CO_2 loading of 0.56 mol_{CO_2} mol_{amine}^{-1} (Fig. 2a). In contrast, the 5 M MDEA, tested at its maximum attainable CO_2 loading of 0.29 mol_{CO_2} mol_{amine}^{-1}, reached only 30% CO FE (Fig. S4).

MEA, a primary amine, captures CO_2 as stable carbamate, whereas MDEA, a tertiary amine, forms bicarbonate (eqn (1) and (2) in Fig. 1). Increasing the MDEA content raises the post-capture bicarbonate concentration. We therefore hypothesized that the higher CO FE observed with higher MDEA content resulted from an increased bicarbonate fraction.[18] To test this hypothesis, we performed thermodynamic calculations, which showed that protonation of bicarbonate is more favorable than that of carbamate (Fig. 2b). Bicarbonate also diffuses faster, with diffusion coefficients of 7×10^{-5} cm^2 s^{-1} compared to 6.8×10^{-6} cm^2 s^{-1} for carbamate.[25,26] These findings suggest

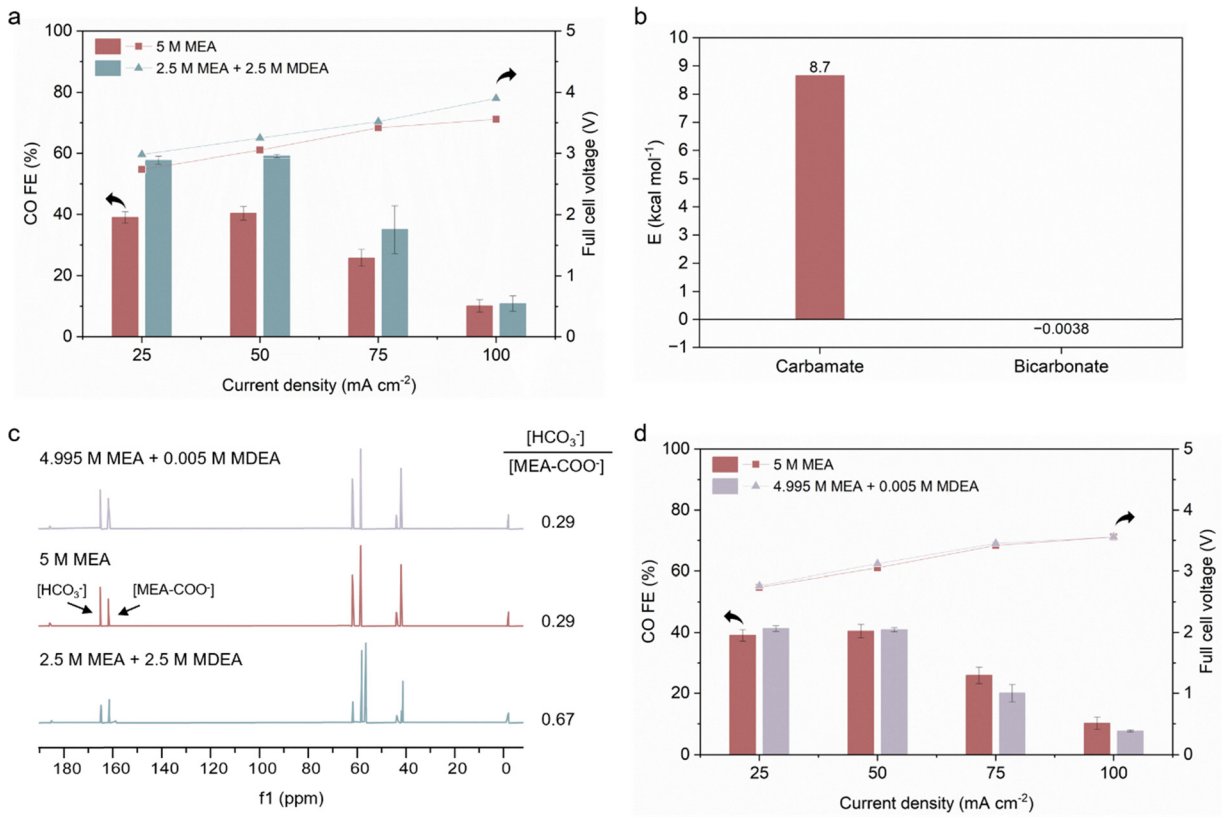

Fig. 2 The effect of post-capture solution composition on electrolysis performance using MEA/MDEA blend. (a) FE towards CO and full cell voltage of 5 M MEA and 2.5 M MEA + 2.5 M MDEA solutions at the same CO_2 loading of 0.56 mol_{CO_2} mol_{amine}^{-1}. (b) Thermodynamic calculations on proton reactions with carbamate and bicarbonate. (c) Quantitative ^{13}C NMR spectra for the post-capture 5 M MEA, 2.5 M MEA + 2.5 M MDEA, and 4.995 M MEA + 0.005 M MDEA solutions at the same CO_2 loading of 0.56 mol_{CO_2} mol_{amine}^{-1}, and the quantified bicarbonate-to-carbamate ratio in each post-capture solution. (d) FE towards CO and full cell voltage of 5 M MEA and 4.995 M MEA + 0.005 M MDEA solutions at the same CO_2 loading of 0.56 mol_{CO_2} mol_{amine}^{-1}.

that the CO_2 regeneration pathway in this system is likely dominated by the proton-assisted conversion of bicarbonate, which is a more thermodynamically favored chemisorbed CO_2 species for regeneration. MEA contributes to fast carbamate-bicarbonate exchange, while MDEA increases the bicarbonate reservoir. Further kinetics analysis would help to quantitatively elucidate this proposed regeneration mechanism in a future study.

Using quantitative carbon-13 nuclear magnetic resonance (^{13}C NMR), we measured the carbamate and bicarbonate concentrations in each solution. In the 5 M MEA solution, the bicarbonate and carbamate concentrations were 0.63 M and 2.14 M, respectively, resulting in a bicarbonate-to-carbamate ratio of 0.29. In the 2.5 M MEA + 2.5 M MDEA solution the bicarbonate and carbamate concentrations were 1.09 M and 1.67 M, respectively, resulting in a ratio of 0.67 (Fig. 2c). This increase in bicarbonate content correlates with the observed improvement in CO FE.

To isolate the potential effect of MDEA addition on electrolysis performance, we varied the molar ratio of MEA to MDEA to produce a 5 M blend with the same bicarbonate-to-carbamate ratio as 5 M MEA. This was possible because MDEA in the blend promotes both carbamate formation (by shifting MEA equilibrium) and bicarbonate formation (*via* direct CO_2 reaction).[27] We identified that a 4.995 M MEA + 0.005 M MDEA blend produces the same bicarbonate-to-carbamate ratio (0.29) as the 5 M MEA reference (Fig. 2c and Fig. S5). With this matching ratio and CO_2 loading, the MEA/MDEA blend performed similarly to the 5 M MEA solution across all current densities (Fig. 2d). This result supports the hypothesis that the improved performance observed in MEA/MDEA mixtures stemmed from the higher bicarbonate fraction, and that the added MDEA does not provide additional improvement in CO FE beyond its role in modifying solution speciation.

Optimal composition of MEA/MDEA solution under industrial CO_2 capture conditions

With the established link between post-capture bicarbonate concentration and electrolysis performance, we next investigated how the initial amine blend composition affects both CO_2 absorption behavior and electrolysis compatibility. Specifically, we aimed to identify blend ratios that balance (i) fast CO_2 absorption kinetics and high loading capacity at industrial capture conditions for high capture efficiency with (ii) high bicarbonate concentration which enhances CO_2 availability for high CO FE.

We evaluated a series of MEA/MDEA blends under simulated industrial CO_2 absorption conditions. The blends, spanning from pure MEA to 1 M MEA + 4 M MDEA, were placed in a 40 °C water bath and exposed to a simulated flue gas stream (15 vol% CO_2 balanced with N_2) at 1 atm. We measured the CO_2 loading capacity of each blend and modelled it using ASPEN HYSYS under the same conditions (Fig. 3a and Fig. S6, S7). The 5 M MEA achieved a CO_2 loading of 0.56 mol_{CO_2} mol_{amine}^{-1}, consistent with previous reports and model predictions.[24] Both experimental and simulation results showed a decreasing trend in CO_2 loading capacity with increasing MDEA content at 40 °C and a CO_2 partial pressure of 0.15 atm, aligning with prior findings under similar conditions.[28,29] We measured the CO_2 absorption kinetics of each solution through the time it took to reach their respective CO_2 loading capacity (Fig. S8). Overall, the 5 M MEA exhibited the best absorption performance, closely followed by the 4 M MEA + 1 M MDEA, while the blends with higher MDEA ratios showed both slower CO_2 absorption rate and lower CO_2 loading capacity (Fig. 3a and Fig. S8).

Recognizing that industrial absorbers typically operate below full capacity, we assessed electrolysis performance at 85% of each blend's maximum CO_2 loading capacity—typical of industrial practice.[30,31] Using ^{13}C NMR, we quantified the bicarbonate concentration in each post-capture solution at this loading (Fig. 3b). Despite the decreasing CO_2 loading capacity with increasing MDEA content (less bicarbonate and carbamate concentrations in total), the bicarbonate concentration in the post-capture solutions increased, potentially offering more readily convertible CO_2 species for electrolysis. However, among the blends, the 4 M MEA + 1 M MDEA achieved the highest CO FE at 50 mA cm^{-2} and 75 mA cm^{-2}, despite having lower post-capture bicarbonate concentration than the 1 M MEA + 4 M MDEA blend (Fig. 3c). This result indicates that additional factors beyond bicarbonate concentration may influence performance.

We observed that as MDEA content increases, the solution becomes more resistant to flow. Pure MDEA is ~4.3 times more viscous than pure MEA at room temperature, and increasing MDEA content increases the solution viscosity.[32] We posited that higher viscosity hinders mass transport and reduces ion mobility, potentially limiting CO_2 diffusion to the catalyst surface and thereby lowering CO FE. This reveals a fundamental trade-off in optimizing blend composition: while higher MDEA content increases the post-capture bicarbonate concentration, regenerating more CO_2 for electrolysis, it also slows the transport of bicarbonate and *in situ* regenerated CO_2 through the more viscous medium, reducing CO_2 availability at the catalyst surface. In this context, MEA functions as the "activator", providing rapid CO_2 capture kinetics and high CO_2 loading, whereas MDEA serves as the "promoter", enhancing total bicarbonate concentration at the expense of higher viscosity and slower diffusion. As MDEA content increases, the benefit of higher bicarbonate concentration is offset by hindered CO_2 and ion transport, so the blends with the highest bicarbonate content do not produce the highest CO FE. Instead, the observed maximum in CO FE arises when CO_2 regeneration and transport are co-optimized at intermediate blend compositions.

To understand this trade-off, we developed a multiphysics model to evaluate the CO_2 concentration at the catalyst surface (Tables S1–S4). CO_2 is released at the membrane surface *via* pH swing and diffuse towards the catalyst surface where conversion occurs. The CO_2 diffusion rate for each blend was estimated based on a prior study.[33] Simulation results showed that the 4 M MEA + 1 M MDEA solution achieved an optimal balance between bicarbonate concentration and CO_2 diffusion rate (Fig. 4a), consistent with the experimental observation of its highest CO FE. Interestingly, this blend also aligns with previous reports identifying it as the optimal MEA/MDEA formulation for balancing capture rate and regeneration energy in pilot-scale carbon capture systems.[23]

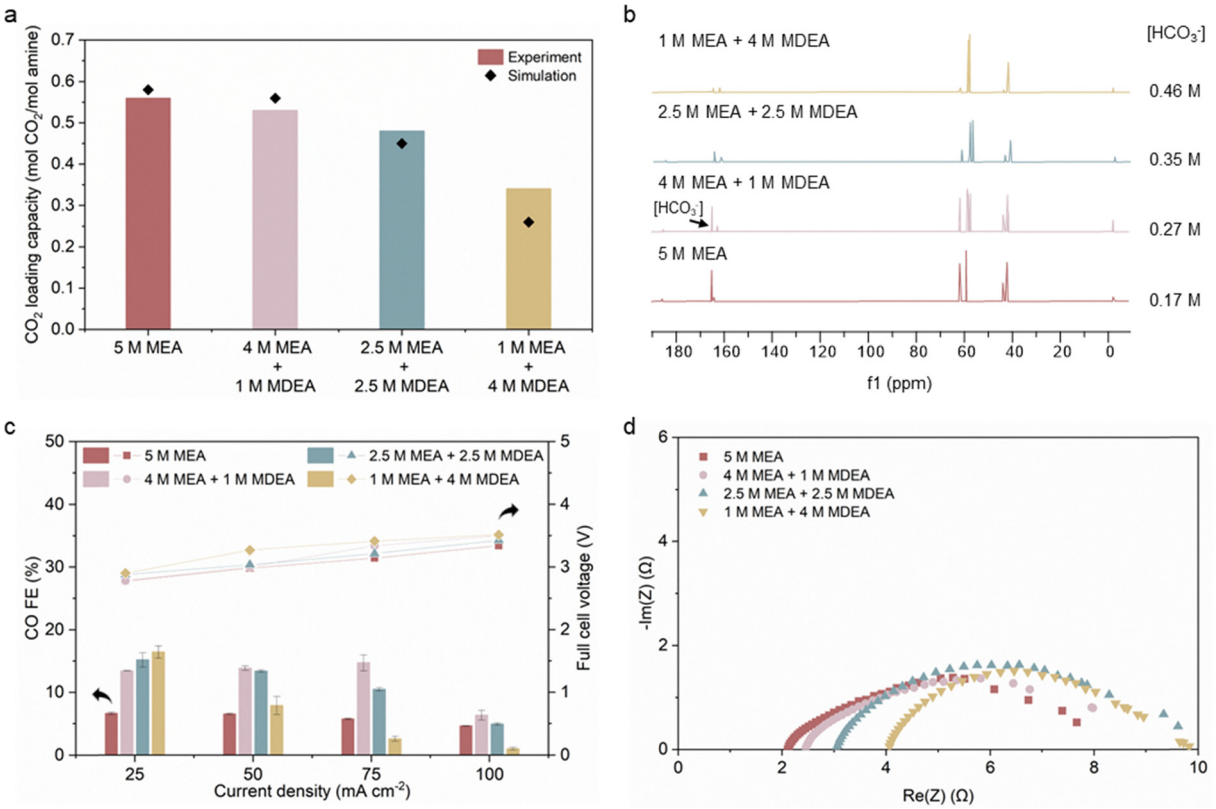

Fig. 3 Optimal composition of MEA/MDEA blend under industrial operating conditions. (a) Experimental and simulated CO_2 loading capacities (mol_{CO_2} mol_{amine}^{-1}) of 5 M MEA and 5 M MEA/MDEA blend solutions capturing at 40 °C and with 15 vol% CO_2 at atmospheric pressure. (b) Quantitative ^{13}C NMR spectra for the post-capture 5 M MEA and 5 M MEA/MDEA blend solutions at 85% of their CO_2 loading capacities measured in (a), and the quantified bicarbonate concentration in each post-capture solution. (c) FE towards CO and full cell voltage of 5 M MEA and 5 M MEA/MDEA blend solutions at 85% of their CO_2 loading capacities measured in (a). (d) Nyquist plots obtained from electrochemical impedance spectroscopy (EIS) for 5 M MEA and 5 M MEA/MDEA blend solutions at 50 mA cm^{-2}.

We also measured the electrolyte conductivity of each solution (Table S5) and performed electrochemical impedance spectroscopy (EIS) at 50 mA cm^{-2} to quantify the series resistance (R_s) during electrolysis (Fig. 3d and Table S5). As MDEA concentration increased, solution conductivity decreased and R_s increased monotonically. This trend aligns with the observed increase in full cell voltage, suggesting that the higher voltage in MDEA-rich blends stems from reduced ionic conductivity.

Therefore, we find that under industrial operating conditions, optimal MEA/MDEA blends must balance the benefits of increased bicarbonate concentration with the drawbacks of higher viscosity and lower conductivity—while still ensuring sufficient CO_2 loading capacity for effective capture. These findings highlight the importance of jointly optimizing capture chemistry and electrolyte properties for high-performance RCC.

Broad applicability of bicarbonate concentration and electrolyte properties on electrolysis performance

To explore whether the correlation between bicarbonate concentration and electrolyte properties on electrolysis performance applies across diverse amine systems, we employed an industrial CO_2 capture blend: ADIP-X, composed of 0.6 M piperazine (PZ) and 3 M MDEA.[34] ADIP-X has a higher CO_2 loading capacity than 5 M MEA under comparable absorption conditions, and improved resistance to thermal and oxidative degradation.[35] At a CO_2 loading of ~0.45 mol_{CO_2} mol_{amine}^{-1}—equivalent to 85% of the CO_2 loading capacity for 4 M MEA + 1 M MDEA under industrial operating conditions (capturing at 40 °C and with 15 vol% CO_2 at atmospheric pressure)—ADIP-X exhibited a CO FE of 36%, compared to 14% for the 4 M MEA + 1 M MDEA blend at 50 mA cm^{-2}, with a similar full cell voltage across all current densities (Fig. 4b).

Quantitative ^{13}C NMR analysis showed a bicarbonate concentration of 1.72 M in the post-capture ADIP-X solution—significantly higher than the 0.27 M in 4 M MEA + 1 M MDEA (Fig. 4c). However, ADIP-X is also ~1.5 times more viscous than the 4 M MEA + 1 M MDEA blend.[36–38] To understand why APID-X outperforms despite its higher viscosity, we revisited the multiphysics model to compare the two systems. In the absence of experimental diffusion data for ADIP-X—likely due to its high viscosity—we approximated the CO_2 diffusion rate using reported values for 40 wt% MDEA solution (~3.5 M MDEA).[39,40] The simulation results show that when the bicarbonate concentration is sufficiently high, the impact of CO_2 diffusivity on electrolysis performance becomes minimal (Fig. 4a).

To enable direct comparison with other RCC studies, typically conducted at full CO_2 saturation, we evaluated both

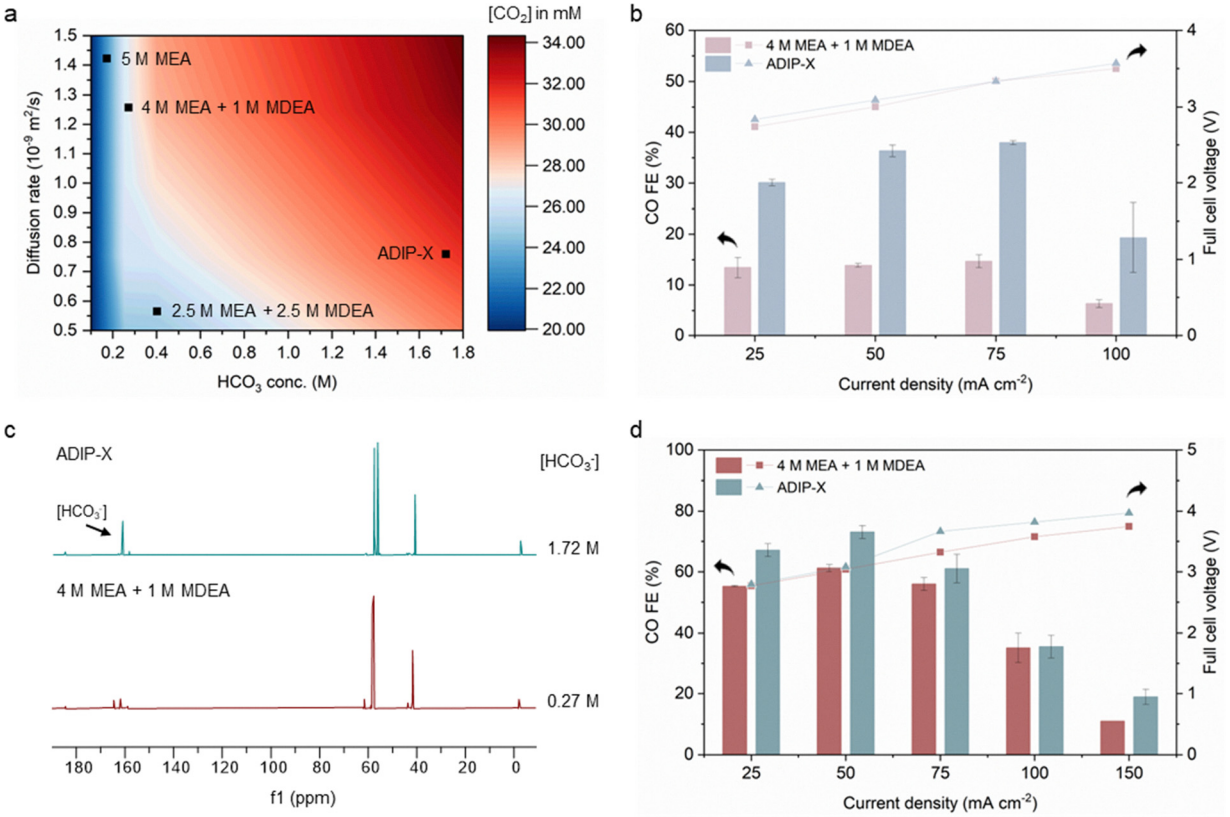

Fig. 4 Comparison of industrial amine blends. (a) Simulation results for CO_2 concentration at the catalyst surface for various MEA/MDEA blends and ADIP-X. (b) FE towards CO and full cell voltage of 4 M MEA + 1 M MDEA and ADIP-X solutions at the same CO_2 loading of 0.45 mol_{CO_2} mol_{amine}^{-1}. (c) Quantitative ^{13}C NMR spectra for the post-capture 4 M MEA + 1 M MDEA and ADIP-X solutions at the same CO_2 loading of 0.45 mol_{CO_2} mol_{amine}^{-1}, and the quantified bicarbonate concentration in each post-capture solution. (d) FE towards CO and full cell voltage of 4 M MEA + 1 M MDEA and ADIP-X solutions at their saturated CO_2 loadings, captured CO_2 at room temperature and with 100 vol% CO_2 at atmospheric pressure.

ADIP-X and 4 M MEA + 1 M MDEA at their respective full CO_2 loading capacities (room temperature, 100 vol% CO_2 at atmospheric pressure). Under these conditions, both solutions exhibited improved performance relative to operation at ~0.45 mol_{CO_2} mol_{amine}^{-1}. ADIP-X again outperformed the 4 M MEA + 1 M MDEA, achieving a CO FE of 73% at 50 mA cm^{-2} with a full cell voltage of 3.1 V, corresponding to an energy efficiency (EE) of 31% towards CO (Fig. 4d). This CO EE marks a 2.4-fold improvement compared to the best reported for single-amine reactive capture systems operating under similar conditions. Preliminary stability tests under these conditions show a gradual decrease in performance over ~10 h of continuous operation (Fig. S9), likely due to amine-induced degradation of the Ni–N/C catalyst.[41] Catalyst durability therefore remains an important area for improvement, and optimized catalyst formulations will enable meaningful regeneration and cycling studies of amine solvents and their blends under electrochemical conditions. Using an established method that accounts for capture and electrolysis,[10] we estimate a total energy demand of 29.8 GJ t^{-1} CO (3.1 V, 50 mA cm^{-2}, 73% CO FE), lower than gas-phase CO_2RR (33.3 GJ t^{-1} CO) and competitive with state-of-the-art reactive capture schemes (30.2 GJ t^{-1} CO), highlighting the potential of amine blends to reduce the overall energy cost of CO production from captured CO_2.

Conclusions

This work demonstrates that amine blends can offer a viable path for reactive CO_2 capture of industrial flue gas, outperforming single amine as well as traditional alkali-based systems. We found that higher post-capture bicarbonate concentrations improve CO FE but must be balanced against viscosity and conductivity. The optimal MEA/MDEA blend achieved this balance, enabling efficient CO_2 capture and conversion. Extending to the industrial ADIP-X blend, we achieved a CO FE of 73% at 50 mA cm^{-2} and a full cell voltage of 3.1 V, corresponding to a CO EE of 31%. Given that industrial absorbers operate at elevated pressures and temperatures, further tuning of amine formulations under these conditions may enable even higher RCC performance. Further catalyst development will be required to achieve improved long-term stability and to enable regeneration and cycling studies of amine solvents and their blends under electrochemical conditions. This work points towards the integration of RCC with existing capture infrastructure to produce renewable CO for downstream fuels and chemicals.

Despite the promising results demonstrated here, several directions for further development remain. (1) Catalyst durability: the Ni–N/C catalyst undergoes gradual deactivation over

~10 h, consistent with nucleophilic amine-reduced degradation. Future work should focus on developing more robust catalysts and evaluating electrode regeneration strategies for long-term operation. (2) Regeneration mechanism: the proton-assisted bicarbonate conversion mechanism is thermodynamically favorable and consistent with the observed dependence of CO FE on bicarbonate fraction, but additional contributions from carbamate-involved routes under certain conditions cannot be excluded. Further kinetic and operando spectroscopic studies will be valuable to quantitatively resolve the regeneration mechanism and to disentangle bicarbonate- and carbamate-mediated contributions. (3) Process engineering considerations: industrial implementation will require evaluation of multi-cycle absorption-electrolysis operation, quantification of amine oxidative degradation, and understanding performance under a variety of absorber-relevant pressures and gas compositions. Incorporating the electrolyte design principles developed here into process-scale studies that quantify amine stability, long-term cycling, and operation at industrial absorber conditions will provide an important next step towards commercialization. (4) Extension to broader amine blends: the activator–promoter framework and the design rule of balancing bicarbonate concentration against viscosity and conductivity are demonstrated here for MEA/MDEA and for ADIP-X (PZ/MDEA). Future work could extend this approach to other industrial blends such as AMP/MDEA, PZ-promoted blends, or sterically hindered amines to establish how broadly this design principle applies and to identify any system-specific refinements. (5) Operation at industrial high current density: the decline in CO FE at 100 mA cm^{-2} indicates unresolved mass-transport and kinetic interactions. Future studies that vary hydrodynamics, cell architecture, and electrolyte properties will be important to identify the rate-limiting steps and to guide operation at higher current densities, providing opportunities to further enhance the practical viability of reactive capture systems.

Methods

Materials

All reagents were purchased from commercial suppliers without further modification, unless otherwise specified. Milli-Q water with a resistivity of 18.2 MΩ cm at 25 °C was used for all experiments.

Ni–N/C catalyst synthesis

To synthesize the Ni–N/C catalyst, 3.39 g of zinc nitrate hexahydrate was first dissolved in 180 mL of methanol. Separately, 3.94 g of 2-methylimidazole was dissolved in another 180 mL of methanol and then added to the zinc nitrate solution. The resulting mixture was stirred continuously at 600 rpm and maintained at 60 °C for 24 h. The ZIF-8 powder was collected by centrifuging the mixture, washing with methanol 3 times, and drying under a vacuum at 60 °C overnight. Subsequently, 100 mg of the synthesized ZIF-8 powder was dispersed in 12 mL of *n*-hexanes and sonicated for 1 h at room temperature to form a homogeneous suspension. Then, 216 μL of 0.125 M nickel(II) nitrate hexahydrate solution was added dropwise to the suspension while sonicating at room temperature. The nickel-doped solution was then centrifuged, washed three times with methanol, and vacuum-dried at 60 °C overnight. Finally, the resulting powder was placed in a tube furnace and pyrolyzed at 900 °C for 2 h under a continuous flow of argon (Ar) gas to obtain the Ni–N/C catalyst.

Ni–N/C catalyst characterization

To identify the catalyst's phase information and crystallinity, XRD was conducted using a Rigaku Miniflex diffractometer equipped with Cu Kα radiation (1.5405 Å). The diffraction patterns were recorded with a step size of 0.2° in 2θ and a scanning rate of 5° per minute. All additional settings were optimized to improve the signal-to-noise ratio. High-resolution transmission electron microscopy (HRTEM), high-angle annular dark-field scanning transmission electron microscopy, and energy dispersive X-ray spectroscopy elemental mapping were performed on a double-corrected Thermo Fisher Scientific Spectra Ultra equipped with both Cs Probe and Image corrector. HRTEM samples were prepared by depositing a Ni–N–C suspension onto a lacey carbon film-coated Cu grid.

Electrolyzer operation and gas analysis

The cathode electrode was prepared by spray-coating the Ni–N/C catalyst ink onto a hydrophilic carbon paper (AvCarb MGL190, Fuel cell store). For a 6.25 cm^2 substrate, the ink was composed of 25 mg of Ni–N/C catalyst and 75 mg of Nafion solution (5 wt%, Fuel Cell Store) dispersed in 2 mL of methanol, followed by 1 h of sonication. The cathode catalyst loading was approximately 1 mg cm^{-2}, and the prepared cathode electrode was used with an exposed area of 1 cm^2. The anode electrode was titanium-supported iridium oxide (Magneto Special Anodes, Evoqua Water Technologies). The cathode and anode were separated by a Nafion membrane (N117, Ion Power), with an additional CO_2 diffusion layer—mixed cellulose ester (MCE) membrane filter (8.0 μm pore size, Millipore Sigma)—placed between the cathode and membrane.

All electrochemical experiments were performed using a membrane electrode assembly (MEA) at room temperature and atmospheric pressure, and data were collected using a potentiostat (Autolab PGSTAT204). In a typical experiment, 75 mL of amine-based capture solution was purged with 15 vol% or 100 vol% CO_2 at room temperature or 40 °C until the desired CO_2 loading was achieved. The headspace of the capture solution was connected to a desiccant (DRIERITE 8 mesh, W.A. Hammond) trap to capture evaporated amines, and the amount of CO_2 absorbed was determined by weighing the solution and desiccant trap before and after purging. The post-capture amine-based solution and 75 mL of 0.05 M sulfuric acid (H_2SO_4) solution were circulated as catholyte and anolyte, respectively, using peristaltic pumps. During electrolyzer operations, the catholyte was continuously purged with Ar gas at 20 sccm. To ensure complete removal of dissolved CO_2 and even mixing of gas products, the first gas sample was taken after 20 min of operation. All reported full cell voltages were not *iR* corrected.

Gas products were analyzed using a gas chromatograph (PerkinElmer Clarus 590) equipped with a thermal conductivity detector and a flame ionization detector. A 1 mL sample of gas was collected from the outlet and injected into the chromatograph for quantification. The FE was then calculated using the following equation:

$$\mathrm{FE}_i\ (\%) = \frac{z_i FP}{RT} \times v_i \times \frac{1}{I} \times 100\%$$

where z_i is the moles of electrons required to produce one mole of product i, F is the Faraday's constant, P is the atmospheric pressure, R is the ideal gas constant, T is the room temperature, v_i is the gas flow rate of product i, and I is the total current.

EIS measurements were acquired in the frequency range of 10^5 to 1 Hz at 50 mA cm^{-2}.

Quantitative ^{13}C NMR

^{13}C NMR spectra were obtained using a 500 MHz Agilent DD2 NMR spectrometer. 1 M 2,2,3,3-D(4)-3-(Trimethylsilyl)propionic acid sodium salt (98+ atom% D, Thermo Scientific Chemicals) diluted with deuterium oxide (99.9 atom% D, Millipore Sigma) was used as internal reference. Samples were prepared in 5 mm NMR tubes with 500 mL deuterium oxide (D_2O) and 100 mL test solution. The following acquisition parameters were used: pulse angle = 45.0°, acquisition time = 10.486 s, delay time = 57.514 s, number of data points = 524 288, number of scans = 128. The data were processed by MestReNova x64.

Thermodynamic calculations

Density functional theory calculations of the reaction pathway was performed with Gaussian 16 program package at wB97XD/aug-cc-pVTZ level of theory using CPCM (water) solvent model.

Aspen HYSYS model

Aspen HYSYS V12.1 was used to simulate an amine-based CO_2 capture process and determine the maximum CO_2 absorption capacity of different amine solutions, including 5 M MEA, 4 M MEA + 1 M MDEA, 2.5 M MEA + 2.5 M MDEA, and 1 M MEA + 4 M MDEA. The Acid Gas–Chemical Solvents property package was selected in Aspen HYSYS, as it supports amine blends, including pure MEA and MEA-MDEA mixtures. The flue gas and amine solution temperatures were set to 40 °C, with an absorber operating pressure of 101.3 kPa and 50 equilibrium stages. The process begins with a flue gas stream containing 15% CO_2 and 85% N_2 entering the absorber from the bottom, while the amine solution is introduced from the top. As the gas flows upward and the amine solution flows downward, CO_2 is absorbed into the liquid phase. The CO_2-rich amine solution then exits from the bottom of the absorber, while the nitrogen-rich gas leaves through the top. The maximum CO_2 absorption capacity was determined by progressively increasing the flue gas flow until the amine solution could no longer absorb additional CO_2. The CO_2 loading was then calculated as the molar ratio of absorbed CO_2 to amine molecules in the solution.

Author contributions

D. S. and R. K. M. supervised the project. S. S. S. and Y. C. X. designed all experiments and drafted the figures. S. S. S. carried out all experiments, analyzed the data, and wrote the manuscript. F. L. developed the multiphysics model and carried out simulations. J. W. designed and carried out the ASPEN HYSYS simulations. Y. C. performed DFT calculations. M. L. and Y. W. assisted with catalyst preparation. M. L. performed XRD analysis. Y. W. carried out STEM characterization. M. F. and Y. G. assisted with experiment design. K. H., P. J. C., and P. E. J. assisted with manuscript editing and provided project guidance from an industry perspective. All authors discussed the results and assisted during manuscript preparation.

Conflicts of interest

The authors declare no competing interests.

Data availability

The supporting data have been included as part of the main article and supplementary information (SI). Supplementary information is available. See DOI: https://doi.org/10.1039/d5ey00333d.

Acknowledgements

We gratefully acknowledge support from Shell Global Solutions International B.V., the Canada Research Chairs Program (CRC-2021-00316), and the Natural Sciences and Engineering Research Council of Canada (NSERC) through the Alliance Program and the Discovery Program, as well as Gaussian Inc., Compute Ontario (https://www.computeontario.ca) and the Digital Research Alliance of Canada (https://www.alliancecan.ca). S. S. S. thanks the Government of Ontario for their support through graduate scholarships. Y. C. X. thanks NSERC and Hatch for their support through graduate scholarships.

References

1 G. Wen, B. Ren, X. Wang, D. Luo, H. Dou and Y. Zheng, *et al.*, Continuous CO_2 electrolysis using a CO_2 exsolution-induced flow cell, *Nat. Energy*, 2022, **7**(10), 978–988, DOI: 10.1038/s41560-022-01130-6.

2 C. G. Okoye-Chine, K. Otun, N. Shiba, C. Rashama, S. N. Ugwu and H. Onyeaka, *et al.*, Conversion of carbon dioxide into fuels—A review, *J. CO2 Util.*, 2022, **62**, 102099. Available from: https://www.sciencedirect.com/science/article/pii/S2212982022002189.

3 F. O. Ochedi, J. Yu, H. Yu, Y. Liu and A. Hussain, Carbon dioxide capture using liquid absorption methods: a review, *Environ. Chem. Lett.*, 2021, **19**, 77–109. Available from: https://link.springer.com/article/10.1007/s10311-020-01093-8.

4 G. T. Rochelle, Amine scrubbing for CO_2 capture, *Science*, 2009, **325**(5948), 1652–1654, DOI: 10.1126/science.1176731.

5 P. Yue, Z. Kang, Q. Fu, J. Li, L. Zhang and X. Zhu, *et al.*, Life cycle and economic analysis of chemicals production via electrolytic (bi)carbonate and gaseous CO_2 conversion, *Appl. Energy*, 2021, **304**, 117768. Available from: https://www.sciencedirect.com/science/article/pii/S0306261921011077.

6 M. Li, E. Irtem, H. Iglesias van Montfort, M. Abdinejad and T. Burdyny, Energy comparison of sequential and integrated CO_2 capture and electrochemical conversion, *Nat. Commun.*, 2022, **13**, 5398, DOI: 10.1038/s41467-022-33145-8.

7 J. E. Huang, F. Li, A. Ozden, A. S. Rasouli, F. P. G. de Arquer and S. Liu, *et al.*, CO_2 electrolysis to multicarbon products in strong acid, *Science*, 2021, **372**(6546), 1074–1078. Available from: https://www.science.org/doi/abs/10.1126/science.abg6582.

8 Y. C. Li, G. Lee, T. Yuan, Y. Wang, D. H. Nam and Z. Wang, *et al.*, CO_2 electroreduction from carbonate electrolyte, *ACS Energy Lett.*, 2019, **4**(6), 1427–1431. Available from: https://pubs.acs.org/doi/abs/10.1021/acsenergylett.9b00975.

9 Y. C. Xiao, C. M. Gabardo, S. Liu, G. Lee, Y. Zhao and C. P. O'Brien, *et al.*, Direct carbonate electrolysis into pure syngas, *EES Catal.*, 2022, **1**, 54–61. Available from: https://pubs.rsc.org/en/content/articlelanding/2023/ey/d2ey00046f#!divAbstract.

10 Y. C. Xiao, S. S. Sun, Y. Zhao, R. K. Miao, M. Fan and G. Lee, *et al.*, Reactive capture of CO_2 via amino acid, *Nat. Commun.*, 2024, **15**, 7849, DOI: 10.1038/s41467-024-51908-3.

11 D. J. D. Pimlott, Y. Kim and C. P. Berlinguette, Reactive carbon capture enables CO_2 electrolysis with liquid feedstocks, *Acc. Chem. Res.*, 2024, **57**(7), 1007–1018, DOI: 10.1021/acs.accounts.3c00571.

12 H. M. Almajed, R. Kas, P. Brimley, A. M. Crow, A. Somoza-Tornos and B. M. Hodge, *et al.*, Closing the loop: unexamined performance trade-offs of integrating direct air capture with (bi)carbonate electrolysis, *ACS Energy Lett.*, 2024, **9**(5), 2472–2483, DOI: 10.1021/acsenergylett.4c00807.

13 A. G. Fink, E. W. Lees, J. Gingras, E. Madore, S. Fradette and S. A. Jaffer, *et al.*, Electrolytic conversion of carbon capture solutions containing carbonic anhydrase, *J Inorg. Biochem.*, 2022, **231**, 111782. Available from: https://www.sciencedirect.com/science/article/pii/S016201342200071X.

14 T. N. G. Borhani, A. Azarpour, V. Akbari, S. R. Wan Alwi and Z. A. Manan, CO_2 capture with potassium carbonate solutions: a state-of-the-art review, *Int. J. Greenhouse Gas Control*, 2015, **41**, 142–162. Available from: https://www.sciencedirect.com/science/article/pii/S1750583615300050.

15 Y. Kim, E. W. Lees, C. Donde, A. M. L. Jewlal, C. E. B. Waizenegger and B. M. W. de Hepcée, *et al.*, Integrated CO_2 capture and conversion to form syngas, *Joule*, 2024, **8**(11), 3106–3125. Available from: https://www.sciencedirect.com/science/article/pii/S254243512400463X.

16 F. Meng, Y. Meng, T. Ju, S. Han, L. Lin and J. Jiang, Research progress of aqueous amine solution for CO_2 capture: a review, *Renewable Sustainable Energy Rev.*, 2022, **168**, 112902. Available from: https://www.sciencedirect.com/science/article/pii/S1364032122007845.

17 K. M. G. Langie, K. Tak, C. Kim, H. W. Lee, K. Park and D. Kim, *et al.*, Toward economical application of carbon capture and utilization technology with near-zero carbon emission, *Nat. Commun.*, 2022, **13**, 7482, DOI: 10.1038/s41467-022-35239-9.

18 A. Gautam and M. K. Mondal, Post-combustion capture of CO_2 using novel aqueous triethylenetetramine and 2-dimethylaminoethanol amine blend: equilibrium CO_2 loading-empirical model and optimization, CO_2 desorption, absorption heat, and ^{13}C NMR analysis, *Fuel*, 2023, **331**(2), 125864. Available from: https://www.sciencedirect.com/science/article/pii/S0016236122026898.

19 G. Lee, Y. C. Li, J. Y. Kim, T. Peng, D. H. Nam and A. Sedighian Rasouli, *et al.*, Electrochemical upgrade of CO_2 from amine capture solution, *Nat. Energy*, 2020, **6**, 46–53. Available from: https://www.nature.com/articles/s41560-020-00735-z#author-information.

20 P. Li, Y. Mao, H. Shin, Q. Yang, X. Cheng and Y. Li, *et al.*, Tandem amine scrubbing and CO_2 electrolysis via direct piperazine carbamate reduction, *Nat. Energy*, 2025, **10**, 1262–1273, DOI: 10.1038/s41560-025-01869-8.

21 J. H. Kim, H. Jang, G. Bak, W. Choi, H. Yun and E. Lee, *et al.*, The insensitive cation effect on a single atom Ni catalyst allows selective electrochemical conversion of captured CO_2 in universal media, *Energy Environ Sci.*, 2022, **15**(10), 4301–4312. Available from: https://pubs.rsc.org/en/content/articlelanding/2022/ee/d2ee01825j.

22 A. Gautam and M. K. Mondal, Review of recent trends and various techniques for CO_2 capture: special emphasis on biphasic amine solvents, *Fuel*, 2023, **334**(1), 126616. Available from: https://www.sciencedirect.com/science/article/pii/S0016236122034408.

23 R. Idem, M. Wilson, P. Tontiwachwuthikul, A. Chakma, A. Veawab and A. Aroonwilas, *et al.*, Pilot plant studies of the CO_2 capture performance of aqueous MEA and mixed MEA/MDEA solvents at the University of Regina CO_2 Capture Technology Development Plant and the Boundary Dam CO_2 Capture Demonstration Plant, *Ind. Eng. Chem. Res.*, 2005, **45**(8), 2414–2420, DOI: 10.1021/ie050569e.

24 P. Galindo, A. Schäffer, K. Brechtel, S. Unterberger and G. Scheffknecht, Experimental research on the performance of CO_2-loaded solutions of MEA and DEA at regeneration conditions, *Fuel*, 2012, **101**, 2–8. Available from: https://www.sciencedirect.com/science/article/pii/S0016236111000639.

25 S. E. Jerng and B. M. Gallant, Electrochemical reduction of CO_2 in the captured state using aqueous or nonaqueous amines, *iScience*, 2022, **25**(7), 104558. Available from: https://www.sciencedirect.com/science/article/pii/S2589004222008306.

26 R. E. Zeebe, On the molecular diffusion coefficients of dissolved CO_2, HCO_3^-, and CO_3^{2-} and their dependence on isotopic mass, *Geochim. Cosmochim. Acta*, 2011, **75**(9), 2483–2498. Available from: https://www.sciencedirect.com/science/article/pii/S0016703711000895.

27 R. Zhang, Z. Liang, H. Liu, W. Rongwong, X. Luo and R. Idem, *et al.*, Study of formation of bicarbonate ions in CO_2-loaded aqueous single 1DMA2P and MDEA tertiary amines and blended MEA–1DMA2P and MEA–MDEA amines for low heat of regeneration, *Ind. Eng. Chem. Res.*, 2016, **55**(12), 3710–3717, DOI: 10.1021/acs.iecr.5b03097.

28 Y. Li and A. E. Mather, Correlation and prediction of the solubility of carbon dioxide in a mixed alkanolamine solution, *Ind. Eng. Chem. Res.*, 1994, **33**(8), 2006–2015. Available from: https://pubs.acs.org/doi/10.1021/ie00032a017.

29 D. M. Austgen, G. T. Rochelle and C. C. Chen, Model of vapor-liquid equilibria for aqueous acid gas-alkanolamine systems. 2. Representation of hydrogen sulfide and carbon dioxide solubility in aqueous MDEA and carbon dioxide solubility in aqueous mixtures of MDEA with MEA or DEA, *Ind. Eng. Chem. Res.*, 1991, **30**(3), 543–555, DOI: 10.1021/ie00051a016.

30 S. Orangi, S. Aromada, N. Razi and L. E. Øi, Simulation and economic analysis of MEA + PZ and MDEA + MEA blends in post-combustion CO_2 capture plant, in *Scandinavian Simulation Society*, ed. E. Juuso, B. Lie, E. Dahlquist and J. Ruuska, 2022, pp. 317–324, DOI: 10.3384/ecp21185317.

31 S. Hjelmaas, E. Storheim, N. E. Flø, E. S. Thorjussen, A. K. Morken and L. Faramarzi, *et al.*, Results from MEA amine plant corrosion processes at the CO_2 Technology Centre Mongstad, *Energy Proc.*, 2017, **114**, 1166–1178. Available from: https://www.sciencedirect.com/science/article/pii/S1876610217314613.

32 U. Arachchige, N. Aryal, D. A. Eimer and M. C. Melaaen, Viscosities of pure and aqueous solutions of monoethanolamine (MEA), diethanolamine (DEA) and *N*-methyldiethanolamine (MDEA), *Annu. Trans. Nord. Rheol. Soc.*, 2013, **22**, 299–306. Available from: https://www.researchgate.net/publication/303157751_Viscosities_of_Pure_and_Aqueous_Solutions_of_Monoethanolamine_MEA_Diethanolamine_DEA_and_N-Methyldiethanolamine_MDEA.

33 M. Li and M. Lai, Solubility and diffusivity of N_2O and CO_2 in (monoethanolamine + *N*-methyldiethanolamine + water) and in (monoethanolamine + 2-Amino-2-methyl-1-propanol + water), *J. Chem. Eng. Data.*, 1995, **40**(2), 486–492, DOI: 10.1021/je00018a029.

34 M. Dharwadkar, J. Leontowich and A. Spence, Technology selection report-capture 07-0-PX-0580-0001. 2010 Nov [cited 2025 Aug 28]. Available from: https://open.alberta.ca/dataset/46ddba1a-7b86-4d7c-b8b6-8fe33a60fada/resource/b3b052a0-b2ef-4cfc-95b1-b363b9272546/download/technology_selection_report.pdf.

35 F. Closmann, T. Nguyen and G. T. Rochelle, MDEA/Piperazine as a solvent for CO_2 capture, *Energy Proc.*, 2009, **1**(1), 1351–1357. Available from: https://www.sciencedirect.com/science/article/pii/S1876610209001787.

36 U. S. P. R. Arachchige, Viscosity of aqueous solutions of *N*-methyldiethanolamine + monoethanolamine (MDEA + MEA), *IJSTR*, 2019, **8**(6), 11–15. Available from: https://www.ijstr.org/final-print/june2019/Viscosity-Of-Aqueous-Solutions-Of-N-methyldiethanolamine-Monoethanolamine-mdeamea.pdf.

37 N. B. Kummamuru, Z. Idris and D. A. Eimer, Viscosity measurement and correlation of unloaded and CO_2-loaded aqueous solutions of *N*-methyldiethanolamine-piperazine, *J. Chem. Eng. Data*, 2019, **64**(11), 4692–4700, DOI: 10.1021/acs.jced.9b00021.

38 P. W. J. Derks, E. S. Hamborg, J. A. Hogendoorn, J. P. M. Niederer and G. F. Versteeg, Densities, viscosities, and liquid diffusivities in aqueous piperazine and aqueous (piperazine + *N*-methyldiethanolamine) solutions, *J. Chem. Eng. Data*, 2008, **53**(5), 1179–1185, DOI: 10.1021/je800031p.

39 H. A. Al-Ghawas, D. P. Hagewiesche, G. Ruiz-Ibanez and O. C. Sandall, Physicochemical properties important for carbon dioxide absorption in aqueous methyldiethanolamine, *J. Chem. Eng. Data*, 1989, **34**(4), 385–391, DOI: 10.1021/je00058a004.

40 H. M. Polat, C. van der Geest, F. de Meyer, C. Houriez, T. J. H. Vlugt and O. A. Moultos, Densities, viscosities, and diffusivities of loaded and unloaded aqueous CO_2/H_2S/MDEA mixtures: a molecular dynamics simulation study, *Fluid Phase Equilib.*, 2023, **575**, 113913. Available from: https://www.sciencedirect.com/science/article/pii/S0378381223001930.

41 R. E. Siegel, S. Pattanayak and L. A. Berben, Reactive Capture of CO_2: Opportunities and Challenges, *ACS Catal.*, 2022, **13**(1), 766–784, DOI: 10.1021/acscatal.2c05019.